



Multiphysics simulation of the resistance spot welding detection using electromagnetic ultrasonic transverse wave

Shanyue Guan^{1,2} · Ximing He^{1,2} · Xiaokai Wang^{1,2} · Lin Hua^{1,2}

Received: 24 June 2019 / Accepted: 21 July 2020 / Published online: 9 August 2020
© Springer-Verlag London Ltd., part of Springer Nature 2020

Abstract

Resistance spot welding (RSW) quality substantially influences the autobody's mechanical properties and safety performance. Nondestructive testing (NDT) method is widely used to evaluate the quality of RSW, but the traditional ultrasonic testing method has high requirements for coupling conditions and flat surface of the weld part. The electromagnetic acoustic transducer (EMAT) is a novel NDT technology, which has advantages of noncontact, no coupling media, and low requirements for surface flatness of the workpiece. Therefore, the electromagnetic ultrasonic transverse wave (EUTW) is developed to realize the evaluation of RSW quality in this paper. Under the COMSOL platform, the finite element method (FEM) modeling is proposed by multiphysics simulation. The multiphysical fields include electromagnetic field, acoustic field, and solid mechanics. The generation mechanism and propagation rules of EUTW in various spot welds are studied by simulation analysis. The correctness of FEM modeling is validated by EUTW experiments; results show that the experimental waveforms of EUTW are consistent with the simulation waveforms. Finally, an evaluation method of the nugget size of RSW is proposed based on the simulation and experiments analysis of EUTW detection of RSW with different nugget diameter and indentation depth. The approach presented in this paper can provide the theoretical foundation and new method for the noncontact, high efficient, and low-cost detection of RSW quality of the autobody.

Keywords Resistance spot welding · Electromagnetic ultrasonic transverse wave (EUTW) · Multiphysics simulation · Finite element method (FEM)

1 Introduction

Resistance spot welding (RSW) is the most common process for joining thin metal in automotive body structures [1, 2], with a typical family car containing up to 5000 welds [3]. The quality and safety performance of the vehicle is directly determined by RSW quality. Comparing with other NDT

methods, ultrasonic testing technology is much concerned by scholars all over the world for low cost, more convenience, no pollution, and high sensitivity [4], which has been applied to detect the RSW quality. Chen et al. [5] used wavelet packet transform (WPT) analyzing the pulse-echo signals of spot welds to establish the relationship between ultrasonic features and nugget diameter or relevant maximum shear load. Martín et al. [6] used artificial neural networks and classification and regression tree (CART) method [7] to carry out intelligent detection and classify RSW in several quality levels. Moghanizadeh [8] evaluated physical properties such as microhardness of spot welding by attenuation coefficient of ultrasonic testing. Song et al. [9] established the mathematical model of the welds detection based on ultrasonic A-scan and obtained the calculation formula of nugget diameter and attenuation coefficient. Thornton et al. [10] used an ultrasonic C-scan technique that was evaluated for NDT of spot welds of aluminum and obtained credible nondestructive assessments

✉ Xiaokai Wang
wxk0919@whut.edu.cn

¹ Hubei Key Laboratory of Advanced Technology for Automotive Components, Wuhan University of Technology, Wuhan 430070, China

² Hubei Collaborative Innovation Center for Automotive Components Technology, Wuhan 430070, China

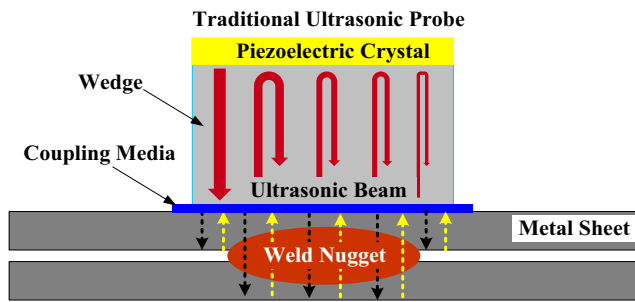


Fig. 1 Traditional ultrasonic detection of RSW

of aluminum weld size and shape. Sun et al. [11] analyzed the mechanical properties of RSW by ultrasonic C-scan imaging.

The above RSW detection methods are based on conventional piezoelectric ultrasonic and their disadvantages are drawn as follows: the entire detection process needs to apply the coupling media, likes shown in Fig. 1, which brings extra procedures and devices, and the body material may be corroded by the residual coupling media. In addition, it requires the higher surface quality of the welded joints; some twisted and rough surfaces of welds affect the ultrasonic propagation, even resulting in nondetectable.

To solve these problems, the EUTW detection of RSW is proposed, which has advantages of noncontact, no coupling media, and low requirements for the workpiece surface. According to the different combination forms of coil and magnet, EUTW can generate different waveforms (such as body wave, surface wave, lamb wave) for different detection objects. The acoustic source profile of spiral coil EUTW is similar to piezoelectric ultrasonic; there are abundant theoretical reports on this kind of EUTW [12–14], and spiral coil EUTW is widely used as an electromagnetic ultrasonic shear wave probe in engineering. The electromagnetic ultrasonic transverse wave generated by the probe propagates along the depth direction of the specimen, and the beam concentrates and directs strongly. Therefore, the simulation and experiment of EUTW are studied to detect the quality of RSW in this paper.

Fig. 2 The generating process of the Lorentz force

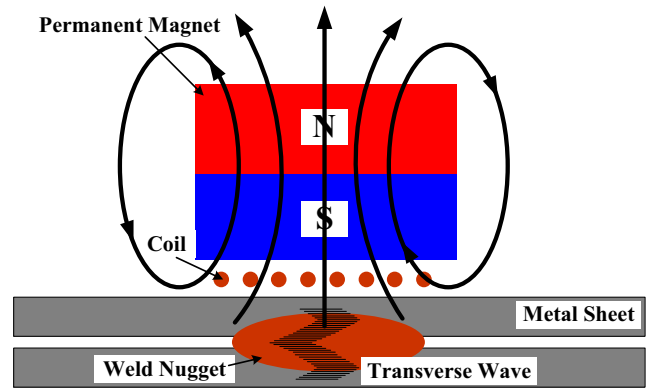
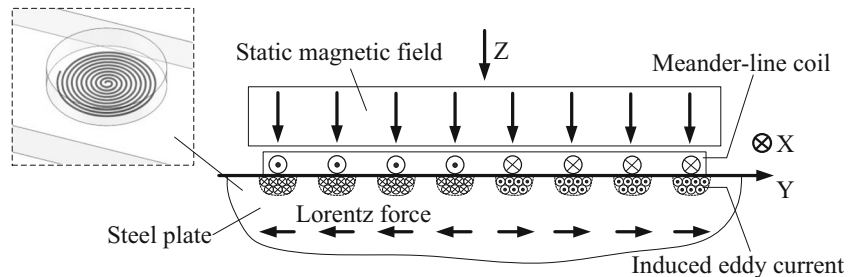


Fig. 3 The schematic diagram of the RSW detection model

2 Basic theory of EUTW multiphysics simulation

There are three kinds of energy exchange mechanisms of EUTW: the Lorentz force mechanism, the magnetostriction force mechanism, and the magnetization force mechanism. The magnetostriction mechanism is the main way for the excitation of ultrasonic waves in a horizontal magnetic field, so the Lorentz force is dominant in a vertical magnetic field. The magnetostriction mechanism is no more than 10%, and the magnetizing force is too small to be neglected [15–23]. In this article, the direction of the static bias magnetic field is perpendicular to the surface of the metal sample, so the Lorentz force mechanism plays a major role. The generating principle of EUTW is shown in Fig. 2.

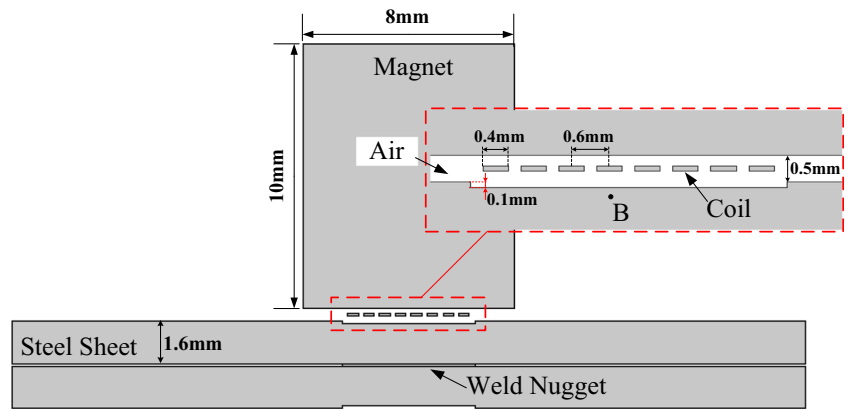
The Lorentz force is the acoustic source of the elastic medium; the linear equation of the acoustic field in an isotropic solid medium is expressed as [24].

$$\rho \frac{\partial^2 \mu}{\partial t^2} = (\lambda_m + 2\mu_m) \nabla(\nabla \cdot \mu) - \mu_m \nabla \times \nabla \times \mu + f_L \tag{1}$$

where ρ is for medium density, μ is for particle displacement, and λ_m, μ_m are the lame constant; f_L is the Lorentz force density.

The receiving process of ultrasonic waves is the inverse process of the generation: when the ultrasonic waves

Fig. 4 The geometric model of electromagnetic ultrasonic testing RSW



propagate to the receiving probe of EMAT, the motion of charged particles in the steel sheet forms a dynamic current under the external static magnetic field [25]. In an EMAT detector, the current density is

$$J = \sigma(\nu \times B) \tag{2}$$

where J is the current density in the conductor, ν is the velocity of the particles which interacts with the magnetic field B , and σ is the conductivity of the material. The dynamic current can produce an alternating magnetic field around the conductor; meanwhile, the EMAT receiving coil in the dynamic magnetic field will generate an induced electromotive force.

3 Establishment of simulation model

The transducer model is simplified in previous studies where assume that the static magnetic field is well-distributed [26–28] and ignores the influence of alternating magnetic field [29–31], or merely modeling the intermediate energy transfer processes, such as eddy current field and magnetic field [32]. In this paper, COMSOL Multiphysics fields coupling calculation software is used for the numerical simulation of EUTW detection of RSW. The static magnetic field, the alternating magnetic field, the solid mechanics field, and the acoustic field are coupled in the EMAT model. Figure 3 depicts the schematic diagram of the RSW detection model.

Table 1 Parameters of the steel sheet

Parameter name	Value	Parameter name	Value
Length	30 mm	Conductivity	$4.032 \times 10^6 \text{ S/m}$
Thickness	1.6 mm	Elastic modulus	205Gpa
Poisson's ratio	0.28		

Due to the excitation and propagation of EUTW involves multiphysical field, the associated coupling variables need to be set in COMSOL software. The body load is defined as multiplying the magnetic flux density by the induced eddy density. The product of the magnetic flux density, the electrical conductivity of steel, and particle's velocity is taken as the source current density of the pulse vortex field to obtain the signal characteristics when calculating the ultrasonic signal received by the coil.

3.1 Building geometric model

According to the structural features of RSW, a two-dimensional model is created, as shown in Fig. 4. In this model, the thickness of the upper and the lower plates is 1.6 mm. A static bias magnetic field, provided by a cylindrical magnet with a diameter of 8 mm, is directed into the steel sheet. The material of permanent magnet is NdFeB, and the coercive force is 915 kA/m. The distance between the bottom of the coil and the upper surface of the steel sheet is 0.2 mm, and the spiral coil is made from 0.4-mm wide copper wire. The number of coil turns is 4 and the distance between two turns is 0.6 mm. Table 1 lists the parameters of the steel sheet.

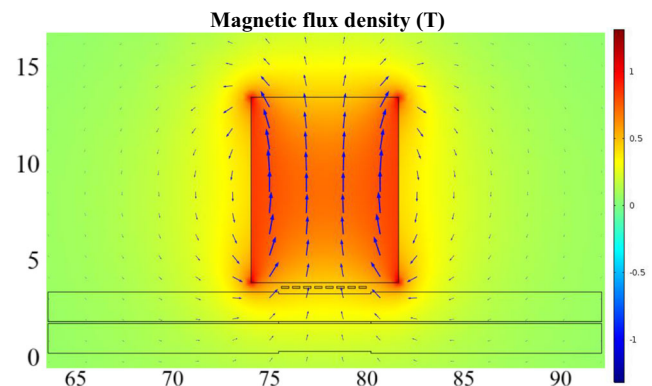


Fig. 5 Static magnetic induction intensity cloud map of a permanent magnet

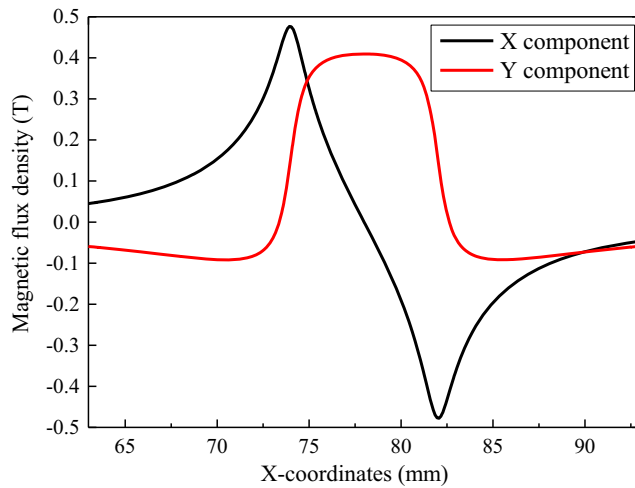


Fig. 6 X, Y component of static magnetic induction intensity

3.2 Simulation analysis of static bias magnetic field

The simulation parameters and boundary conditions are set up to solve the static bias magnetic field; static magnetic induction intensity cloud map of the permanent magnet is shown in Fig. 5. The magnetic induction intensity generated by the permanent magnet edge is the largest; in contrast, the magnetic induction intensity in the middle region is weaker.

Figure 6 shows the static magnetic induction intensity of the X direction and Y direction generated by the permanent magnet respectively. The magnetic induction intensity in the X direction is symmetrically distributed in the center; the value at the center position is zero; the value increases along the two sides and reaches the maximum at the edge, then gradually decreases. The magnetic induction in the Y direction is approximately equal in the central area, and the position of the coil can be considered as a uniform magnetic field.

3.3 Mesh generation

When a high-frequency alternating current is driven through the coil, the induced eddy currents are generated within the

Fig. 7 The result of mesh generations

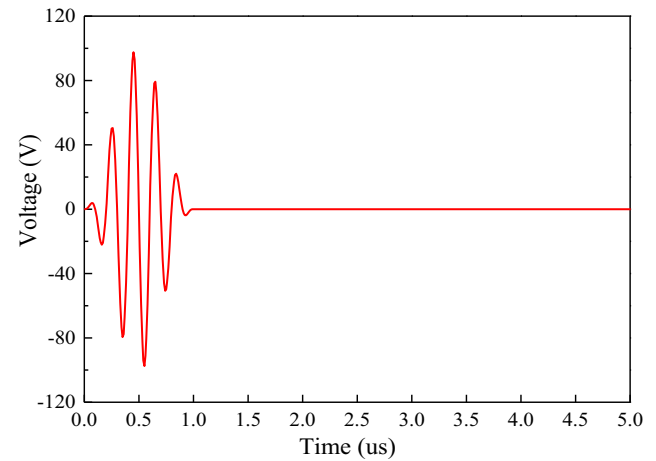
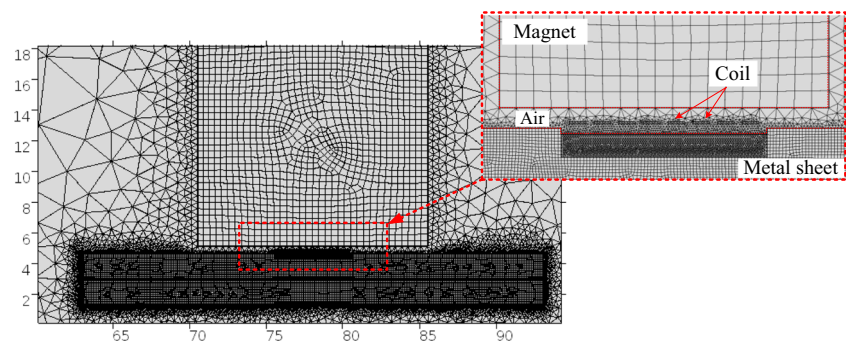


Fig. 8 The waveform of the excitation signal

skin depth of the steel sheet, the electromagnetic ultrasonic energy exchange process is mainly concentrated in this area. To enhance the precision of numerical calculation, the meshes of the energy exchange area need to be refined; the skin depth of steel is expressed as

$$\delta = \frac{1}{\sqrt{\pi f \sigma \mu_0 \mu_r}} \quad (3)$$

where f is excitation current frequency, $f = 5$ MHz, σ is the conductivity of steel, $\sigma = 4.032 \times 10^6$ S/m, μ_0 is vacuum permeability, $\mu_0 = 4\pi \times 10^{-7}$ H/m, μ_r is relative permeability of steel, $\mu_r = 1$.

According to the Eq. (3), the skin depth of steel is calculated to be 112.5 μm , take 5 times of skin depth as the mesh refinement layer of the steel sheet. In dealing with the simulation of the ultrasonic wave, the largest mesh size is usually restricted between 1/10 and 1/5 of the wavelength; this principle cannot only get enough high precision but also avoid the problems of slow solving speed caused by too close meshing or the computer running out of memory [33]. In this model, the meshing size of the refinement layer is less than 1/12 wavelength; other parts of the steel sheet adopt quadrilateral meshes, and their sizes are less than 1/8 of a wavelength; the air domain is divided into triangular meshes by free division.

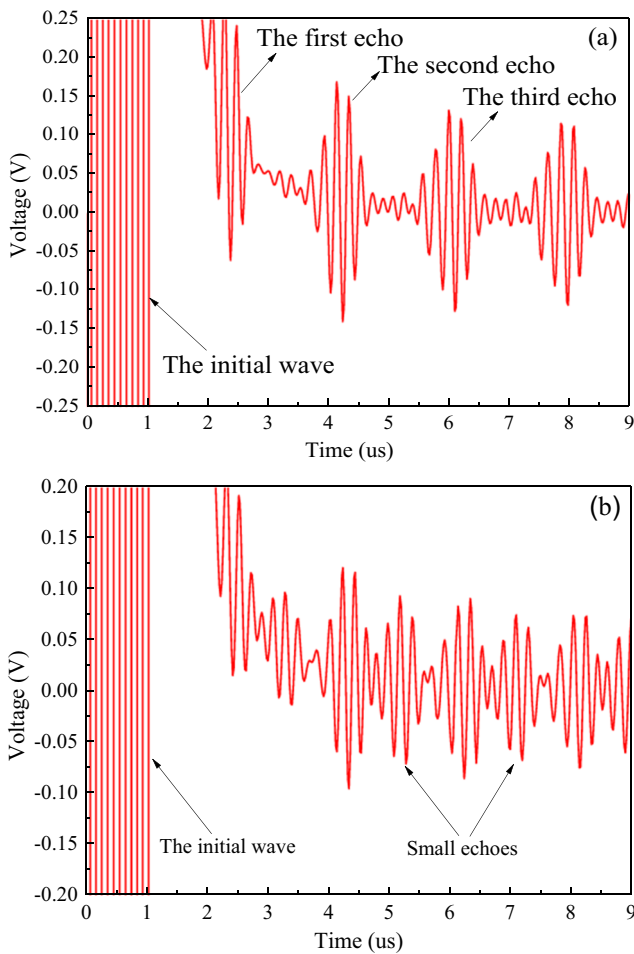


Fig. 9 EUTW simulation signals of spot welds. a Good weld. b Undersize weld

After construction, the total element of the model is 34.263; the result of mesh generations is shown in Fig. 7.

3.4 Selection of excitation signal

In this simulation model, the transient drive pulse is selected as simulating the ultrasonic wave; the excitation signal is modulated through the corresponding Hanning window function, and it is expressed as:

$$(t) = \begin{cases} I \sin(\omega t) \times \left(1 - \cos\left(\frac{\omega t}{n}\right)\right) & 0 \leq t \leq (2n\pi)/\omega \\ 0 & t > (2n\pi)/\omega \end{cases} \quad (4)$$

Fig. 10 Undersize the weld distribution diagram of the particle displacement in the X-direction. a 0.4 μs. b 0.8 μs. c 1.2 μs. d 1.8 μs

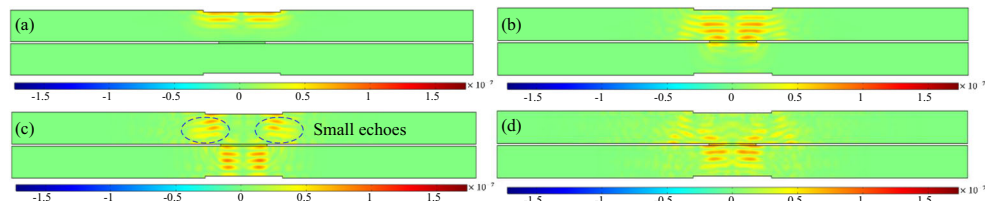


Fig. 11 The electromagnetic ultrasonic testing equipment

where n is the number of pulse signal cycle, $\omega = 2\pi f$, f is the frequency of the excitation current and I is the magnitude of the excitation current, in this study: $f = 5 \text{ MHz}$, $n = 5$, $I = 50 \text{ A}$. Figure 8 displays the ultrasonic waveform of the excitation signal.

In this model, the nugget diameter of the good weld is 5 mm, and the indentation depth is 0.1 mm, and the diameter of indentation is set to the same as the nugget. The nugget diameter of an undersized weld is 3 mm; EUTW simulation signals of the two models are shown in Fig. 9.

A model of the undersize weld is simulated and obtain the distribution of the particle displacement in the X direction is obtained as shown in Fig. 10. It is found that a part of the initial waves reflects on the bottom of the upper plate; the others propagate through the weld into the lower plate and reflect on the bottom. It is obvious in Fig. 10c; the small echoes appear between successive back wall echoes.

4 Experimental verification

To validate the correctness of the simulation signals, the EUTW testing experiments are carried out. The 1.6-mm thick dual-phase steel DP590 is used in the experiment, and material properties are the same as that of the simulation model. As is shown in Fig. 11, the electromagnetic ultrasonic testing equipment is a high-power ultrasonic detector PREMAT-

Table 2 Electromagnetic ultrasonic testing parameters

Parameter name	Frequency	Voltage	Sampling time	Repeat frequency
Value	5 MHz	1200 V	9us	200 Hz

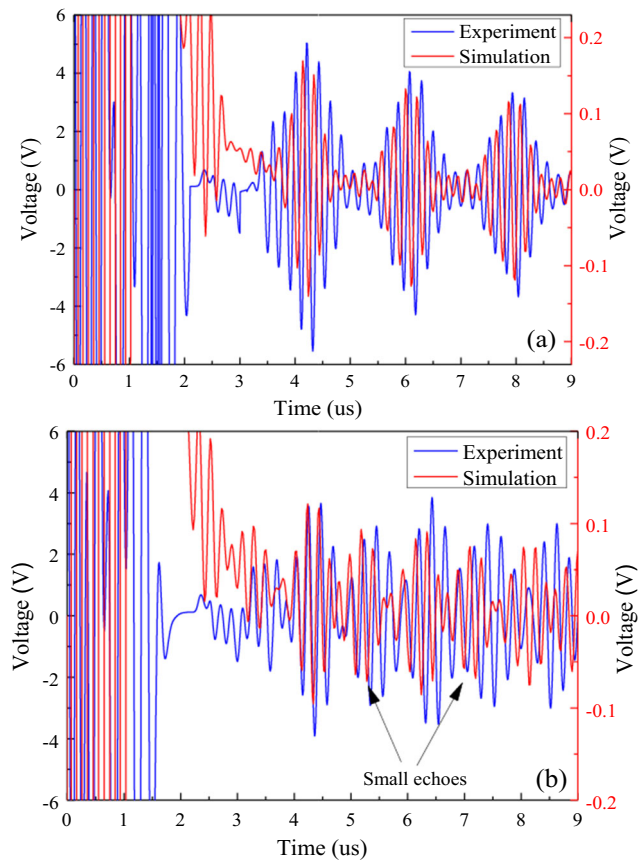
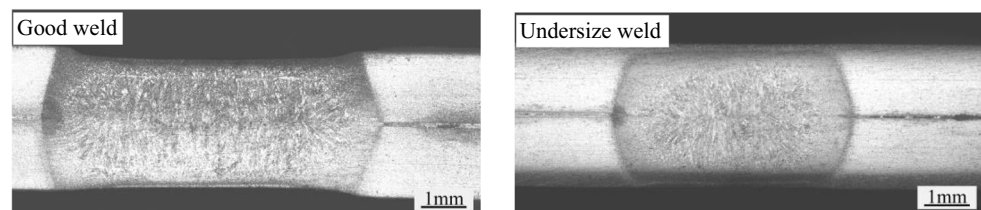
HS200. The electromagnetic ultrasonic probe has a diameter of 10 mm, and its internal coil is 5 mm in diameter. It can be seen in Table 2 that there are electromagnetic ultrasonic testing parameters.

By adjusting the welding parameters and welding conditions, the different types of welded specimens are prepared and, through the metallographic experiment, Fig. 12 show the macrographs of different types of welds.

As is shown in Fig. 13, the detection waveform of both experiment and simulation of a good weld and undersize weld. Compared with the simulation signals, we can find that the time-domain waveforms and the features of both experiments and simulations are very consistent. The only difference is the width of the wavepacket, mainly because the excitation current signals are generated by the transient drive pulse in simulation; meanwhile, the oscillation of the current will enlarge the width of the wavepacket in actual excitation process. In a word, the correctness of the FEM modeling of EMAT detection of RSW is validated.

5 Evaluation of nugget size using EUTW

The weld nugget size is the controlling factor of ultimate tensile shear strength and the resulting spot weld failure modes, it is usually used as the criterion to judge the qualification of RSW in the industry [34]. The larger the nugget size, the higher the strength of the RSW structure, so it is significant to estimate the nugget size by EUTW. As shown in Fig. 14, the size of the nugget area is mainly determined by nugget diameter d and nugget thickness S , and the nugget thickness S equals plate thickness L minus indentation depth h ($S = L - 2h$). Therefore, the detection of nugget diameter d and indentation depth h is the key to evaluate the quality of RSW. In this paper, the evaluation method of nugget diameter d and

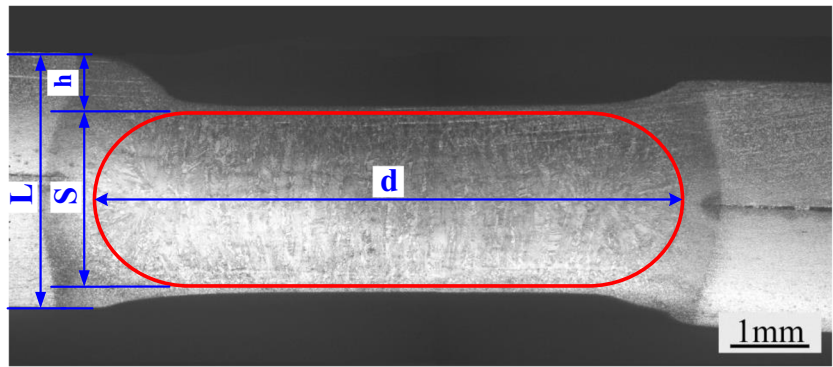
Fig. 12 Macrographs of good weld and undersize weld**Fig. 13** The detection signals of both experiment and simulation. **a** Good weld. **b** Undersize weld

indentation depth h are studied respectively by using the EUTW simulation and experimental signals, which provides theoretical value for the size evaluation of the nugget area.

5.1 Evaluation of nugget diameter using EUTW

The size of the nugget diameter in RSW mainly affects the reflected echo amplitude of the ultrasonic wave on the bottom of the upper plate. As shown in Fig. 15, the reflected echo amplitude of the air layer on the bottom of the upper plate is $|P_1|$, the echo amplitude reflected by ultrasound through the nugget at the bottom of the lower plate is $|P_2|$. So $|P_1|$ decreases with the increase of nugget diameter and while $|P_2|$ is the opposite. To characterize the nugget diameter, the

Fig. 14 The size of the weld nugget area



formula for calculating the amplitude coefficient K is defined as follows:

$$K = \frac{|P_2|}{|P_1|} \tag{5}$$

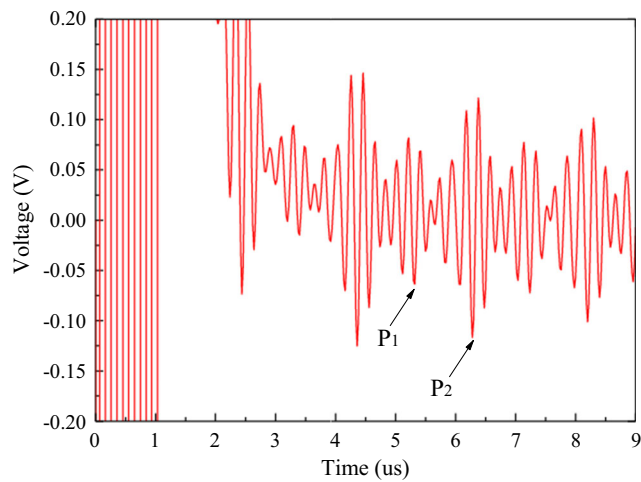


Fig. 15 EUTW simulation signal of RSW with 4-mm nugget diameter

Table 3 Amplitude coefficient of simulation signals with different nugget diameters

Preset nugget diameter d_i (mm)	$ P_1 $	$ P_2 $	K
5.0	0.011	0.128	11.64
4.8	0.023	0.142	6.17
4.5	0.038	0.139	3.66
4.2	0.053	0.127	2.39
4.0	0.064	0.117	1.83
3.8	0.066	0.109	1.65
3.5	0.068	0.104	1.53
3.2	0.069	0.089	1.29
3.0	0.070	0.086	1.23
2.8	0.076	0.085	1.12
2.5	0.079	0.084	1.06
2.2	0.085	0.082	0.96
2.0	0.089	0.077	0.87

By establishing EUTW simulation models of spot welds with various nugget sizes, the transverse wave signals are obtained. To study the relationship between the amplitude coefficient K and the preset nugget diameter d_i , the peak amplitude of the signal is extracted, and the amplitude coefficient K is calculated, as shown in Table 3. When the nugget diameter is very small (< 2 mm), the effect of diffraction on the calculation results of nugget diameter is relatively large, so the nugget can be regarded as a diffraction hole. Most of the energy of sound waves passing through the nugget is diffracted, and only a small part of the energy is received by the probe. As a result, the nugget diameter range of the simulation model is set to 2~5 mm.

Figure 16 illustrates that the nugget diameter d_i is positively correlated with the amplitude coefficient K . The smaller the nugget diameter is, the smaller the amplitude coefficient K is. When the nugget diameter decreases from 5 to 4 mm, the amplitude coefficient K changes dramatically from 11.64 to 1.83, while when the nugget diameter d_i is less than 4 mm, the amplitude coefficient K changes steady. Therefore, the eligibility of the nugget diameter can be judged by the magnitude

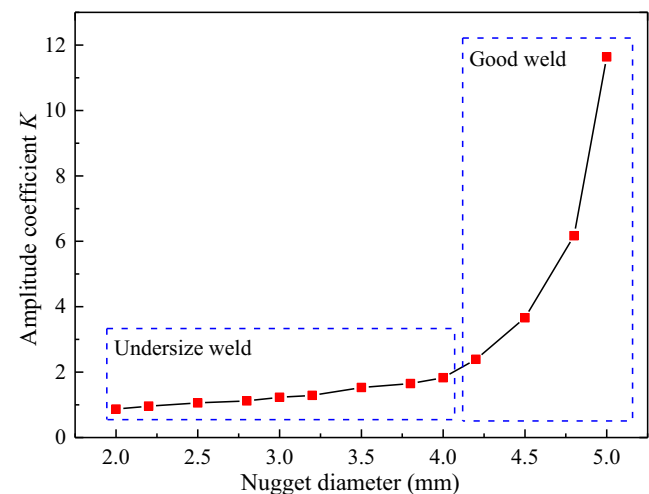


Fig. 16 Curve of amplitude coefficient K with the nugget diameter d_i

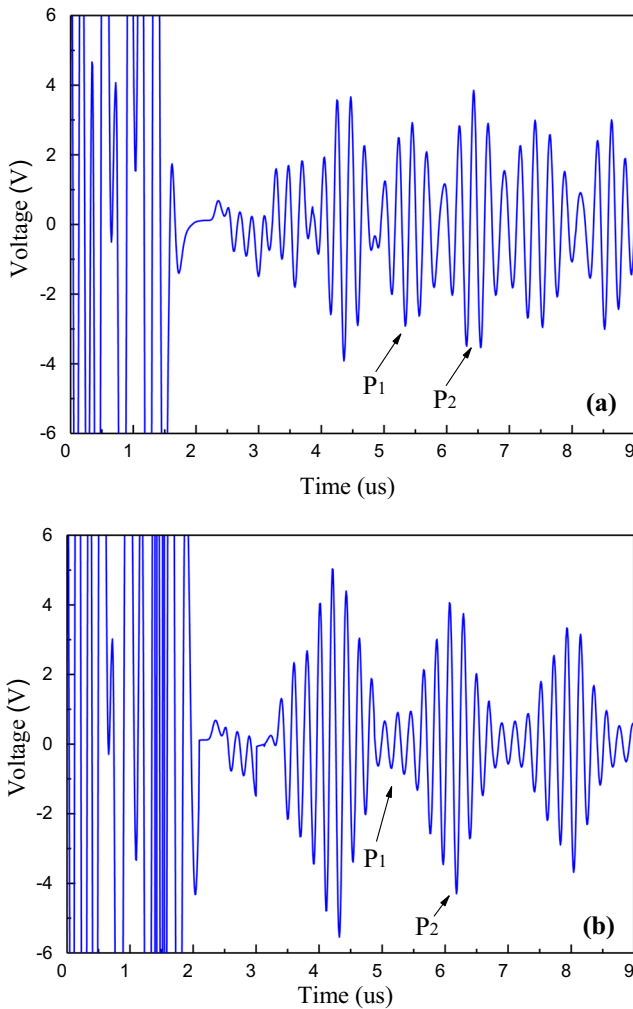


Fig. 17 The experimental signals of EUTW. **a** Unqualified RSW. **b** Qualified RSW

Table 4 Amplitude coefficient of experimental signals with different RSW

No.	Quality of RSW	$ P_1 $	$ P_2 $	K
a	Unqualified RSW	5.358	3.892	0.726
b	Qualified RSW	0.715	4.363	6.102

coefficient. When the magnitude coefficient is less than 2, the unqualified nugget diameter can be judged.

The EUTW experimental signals of unqualified RSW and qualified RSW are shown in Fig. 17. The amplitude

coefficients K of two signals are calculated; the results are displayed in Table 4. The nugget diameter of unqualified RSW is too small, so the amplitude coefficients K is less than 2; on the contrary, the amplitude coefficient of qualified RSW is bigger. This law is the same as the simulation result, so the above simulation law can be verified.

5.2 Calculation of indentation depth using EUTW

In the process of RSW, the indentation depth will increase with the increase of the welding current. When the current increases to a certain value, the depth of indentation will exceed the normal value due to the accumulation of heat, resulting in unqualified RSW. The deep indentation causes a larger distance between the electromagnetic ultrasonic probe and the RSW surface, thus reducing the energy exchange efficiency of EMAT. As shown in Fig. 18b, the transverse waves will produce diffraction and scattering waves at the edge of indentation, which leads to the amplitude of the echo signal attenuates. Figure 19 shows the signal amplitude P_A of 0.3-mm indentation is smaller than the signal amplitude P_B of 0.1-mm indentation.

The models of different indentation depth are studied, and the nugget diameter is 5 mm. As shown in Fig. 19, with the depth of indentation increasing, the time of all the back-wall echoes are advanced. According to the relationship between the time of echo sequence and indentation depth, the formula for calculating indentation depth can be derived, so indentation depth h is defined as:

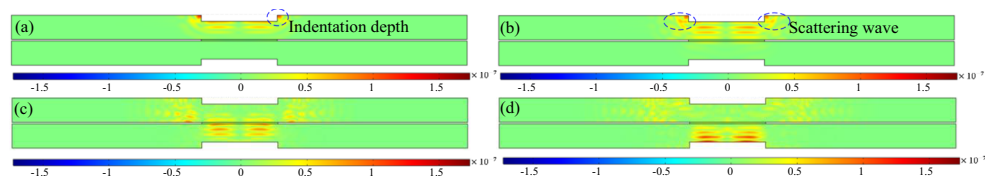
$$h = \frac{L - [(t_2 - t_1) + (t_3 - t_2)]V/4}{2} \tag{6}$$

where L is the thickness of two plates, $L = 3.2$ mm, V is the velocity of the transverse wave in material, $V = 2950$ m/s, t_1 , t_2 , t_3 are three peak times, respectively.

Table 5 shows the calculation results of indentation depth by EUTW simulation signals. Obviously, the calculation values are close to the preset values, and the error is less than 0.05 mm. Therefore, the correctness of the Eq. (6) can be verified.

Two samples of RSW with different indentation depth are detected by EUTW; the experimental signals are shown in

Fig. 18 Deep indentation weld distribution diagram of the particle displacement in the X direction. **a** 0.4 μ s. **b** 0.6 μ s. **c** 1.0 μ s. **d** 1.4 μ s



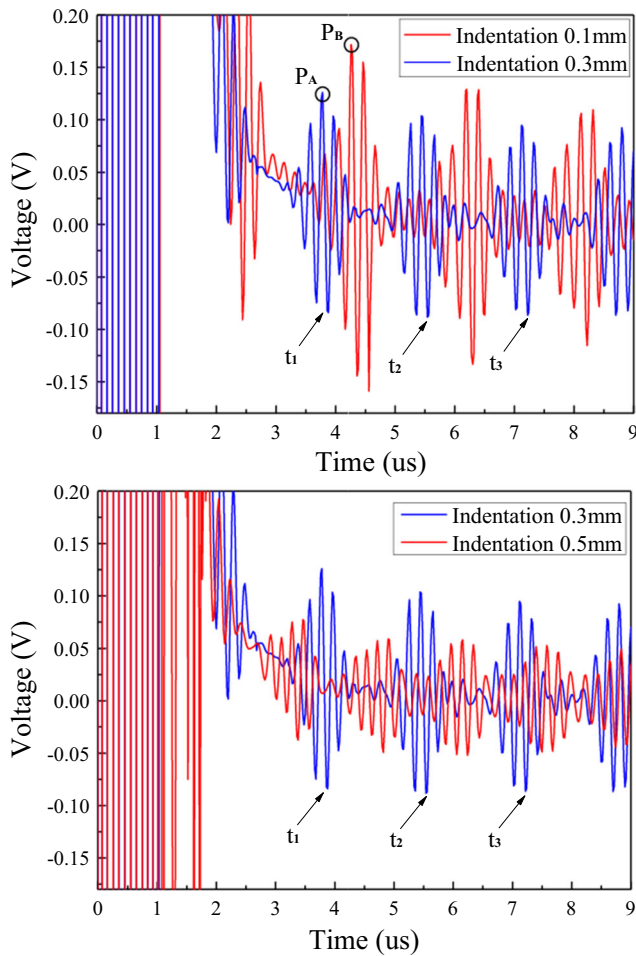


Fig. 19 Simulation signals of RSW with different indentation depth

Fig. 20. The metallographic experiment is used to measure the actual indentation depth of two samples. According to the Eq. (6), the indentation depths are calculated by EUTW experimental signals. It can be seen in Table 6 that the calculation values are close with the actual indentation depth values, and the error is also less than 0.05 mm. It illustrates that EUTW signals of spot welds can effectively calculate indentation

Table 5 Simulation results of the different indentation depth

Preset value h_i (mm)	t_1 (us)	t_2 (us)	t_3 (us)	Calculation value h (mm)	Error (mm)
0.1	4.21	6.19	8.22	0.132	0.032
0.2	3.91	5.82	7.72	0.195	0.005
0.3	3.57	5.33	7.11	0.295	0.005
0.4	3.49	5.14	6.75	0.398	0.002
0.5	3.11	4.56	6.07	0.509	0.009

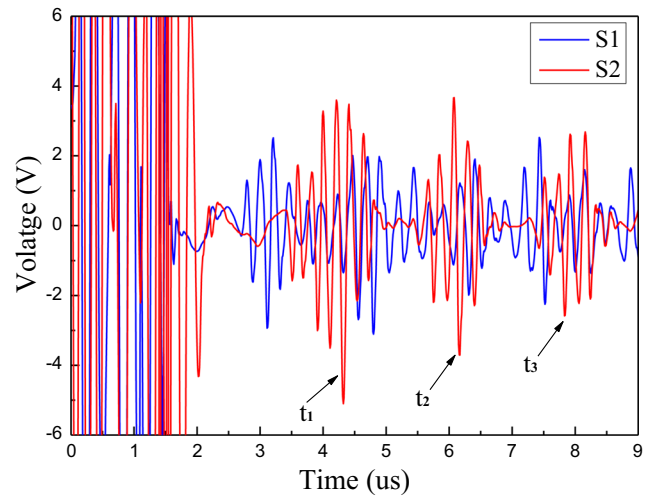


Fig. 20 Experimental signals of RSW with different indentation depth

depth, which has important value for the evaluation of RSW quality.

6 Conclusions

In this paper, we propose a new-coupled electromagnetic-acoustic FEM modeling of the RSW detection in software COMSOL, and the correctness of the simulation method is verified by experiments. In order to evaluate the nugget diameter and indentation depth of RSW, simulation models of different nugget sizes are established, and the changing laws of simulation signals are analyzed. Simulation and analysis show the characteristics of the static bias magnetic field and the generation mechanism and propagation laws of EUTW. Through the EUTW experiments, the different spot welds experimental signals are obtained, and the simulation waveforms are similar to experimental waveforms, which verified the correctness of the modeling method. The characteristics of EUTW simulation signals with various nugget sizes are analyzed to develop the evaluation method of nugget diameter and the calculation method of indentation depth, the calculation error less than 0.05 mm. The effectiveness and calculation accuracy of nugget size evaluation method is verified by sim-

Table 6 Experimental results of the different indentation depth

No.	Actual value h_i (mm)	t_1 (us)	t_2 (us)	t_3 (us)	Calculation value h (mm)	Error (mm)
S1	0.51	3.106	4.582	6.120	0.489	0.021
S2	0.19	4.311	6.164	8.154	0.183	0.007

ulation and experiment signals respectively. EUTW as a non-contact NDT method has a promising application future in detection of RSW quality.

Funding information This work was supported by the National Key R&D Program of China (No. 2018YFB1106500 and No.2019YFB1704500), the National Natural Science Foundation of China (No.51875428), Innovative Research Team Development Program of Ministry of Education of China (No. IRT_17R83) and the 111 Project (No. B17034) of China.

References

- Jou M (2003) Real time monitoring weld quality of resistance spot welding for the fabrication of sheet metal assemblies. *J Mater Process Technol* 132(1–3):102–113
- Lee HT, Wang M, Maev R, Maeva E (2003) A study on using scanning acoustic microscopy and neural network techniques to evaluate the quality of resistance spot welding. *Int J Adv Manuf Technol* 22(9–10):727–732
- Hamidinejad SM, Kolahan F, Kokabi AH (2012) The modeling and process analysis of resistance spot welding on galvanized steel sheets used in car body manufacturing. *Mater Des* 34:759–767
- Liu J, Xu G, Ren L, Qian Z, Ren L (2017) Defect intelligent identification in resistance spot welding ultrasonic detection based on wavelet packet and neural network. *Int J Adv Manuf Technol* 90(9–12):2581–2588
- Chen Z, Shi Y, Jiao B, Zhao H (2009) Ultrasonic nondestructive evaluation of spot welds for zinc-coated high strength steel sheet based on wavelet packet analysis. *J Mater Process Technol* 209(5):2329–2337
- Martín Ó, López M, Martín F (2007) Artificial neural networks for quality control by ultrasonic testing in resistance spot welding. *J Mater Process Technol* 183(2–3):226–233
- Martín Ó, Pereda M, Santos JI, Galán JM (2014) Assessment of resistance spot welding quality based on ultrasonic testing and tree-based techniques. *J Mater Process Technol* 214(11):2478–2487
- Moghanizadeh A (2016) Evaluation of the physical properties of spot welding using ultrasonic testing. *Int J Adv Manuf Technol* 85(1–4):535–545
- Song Y, Hua L, Wang X, Wang B, Liu Y (2016) Research on the detection model and method for evaluating spot welding quality based on ultrasonic A-scan analysis. *J Nondestruct Eval* 35(1):4
- Thomton M, Han L, Shergold M (2012) Progress in NDT of resistance spot welding of aluminium using ultrasonic C-scan. *NDT&E Int* 48:30–38
- Sun X, Zeng K, He X, Zhang L (2017) Ultrasonic C-scan imaging and analysis of the mechanical properties of resistance spot-welded joints of stainless steel. *Nondestruct Test Eva* 32(3):242–254
- Kawashima K (1976) Theory and numerical calculation of the acoustic field produced in metal by an electromagnetic ultrasonic transducer. *J Acoust Soc Am* 60(5):1089–1099
- Garcia-Rodriguez D, Mihalache O, Ueda M (2014) EMAT simulations based on a two-dimensional FEM coupled electro-mechanical formulation. *Int J Appl Electrom* 45(1–4):543–549
- Rosli MH, Edwards RS, Fan Y (2012) In-plane and out-of-plane measurements of Rayleigh waves using EMATs for characterising surface cracks. *NDT&E Int* 49:1–9
- Thompson RB (1990) Physical principles of measurements with EMAT transducers. *Phys Acoust* 19:157–200
- Ribichini R, Cegla F, Nagy PB, Cawley P (2010) Quantitative modeling of the transduction of electromagnetic acoustic transducers operating on ferromagnetic media. *IEEE T Ultrason Ferr* 57(12):2808–2817
- Petcher PA, Potter MDG, Dixon S (2014) A new electromagnetic acoustic transducer (EMAT) design for operation on rail. *NDT&E Int* 65:1–7
- Hirao M, Ogi H (2013) EMATs for science and industry: noncontacting ultrasonic measurements. Springer Science & Business Media
- Ribichini R, Nagy PB, Ogi H (2012) The impact of magnetostriction on the transduction of normal bias field EMATs. *NDT&E Int* 51:8–15
- Ribichini R, Cegla F, Nagy PB, Cawley P (2012) Experimental and numerical evaluation of electromagnetic acoustic transducer performance on steel materials. *NDT&E Int* 45(1):32–38
- Ribichini R, Cegla F, Nagy PB, Cawley P (2011) Study and comparison of different EMAT configurations for SH wave inspection. *IEEE T Ultrason Ferr* 58(12):2571–2581
- Pei C, Zhao S, Xiao P, Chen Z (2016) A modified meander-line-coil EMAT design for signal amplitude enhancement. *Sens Actuators A-Phys* 247:539–546
- Eskandarzade M, Kundu T, Liebeaux N, Placko D, Mobadersani F (2010) Numerical simulation of electromagnetic acoustic transducers using distributed point source method. *Ultrasonics* 50(6):583–591
- Dutton B, Boonsang S, Dewhurst RJ (2006) A new magnetic configuration for a small in-plane electromagnetic acoustic transducer applied to laser-ultrasound measurements: modelling and validation. *Sens Actuators A-Phys* 125(2):249–259
- Mirkhani K, Chaggares C, Masterson C, Jastrzebski M, Dusatko T, Sinclair A, Papini M (2004) Optimal design of EMAT transmitters. *NDT&E Int* 37(3):181–193
- Ludwig R, You Z, Palanisamy R (1993) Numerical simulations of an electromagnetic acoustic transducer-receiver system for NDT applications. *IEEE T Magn* 29(3):2081–2089
- Ludwig R, Dai XW (1991) Numerical simulation of electromagnetic acoustic transducer in the time domain. *J Appl Phys* 69(1):89–98
- Ludwig (1992) Theoretical basis for a unified conservation law description of the electromagnetic acoustic transduction process. *IEEE T Ultrason Ferr* 39(4):476–480
- Ren W, Xu K, Dixon S, Zhang C (2019) A study of magnetostriction mechanism of emat on low-carbon steel at high temperature. *NDT&E Int* 101:34–43
- Jafari-Shapoorabadi R, Konrad A, Sinclair AN (2001) Improved finite element method for EMAT analysis and design. *IEEE T Magn* 37(4):2821–2823
- Jafari-Shapoorabadi R, Konrad A, Sinclair AN (2005) The governing electrodynamic equations of electromagnetic acoustic transducers. *J Appl Phys* 97(10):10E102
- Dutton B, Boonsang S, Dewhurst RJ (2006) Modelling of magnetic fields to enhance the performance of an in-plane EMAT for laser-generated ultrasound. *Ultrasonics* 44:e657–e665
- Liu J, Xu G, Ren L, Qian Z, Ren L (2017) Simulation analysis of ultrasonic detection for resistance spot welding based on COMSOL multiphysics. *Int J Adv Manuf Technol* 93(5–8):2089–2096
- Jagadeesha T (2017) Experimental studies in weld nugget strength of resistance spot-welded 316L austenitic stainless steel sheet. *Int J Adv Manuf Technol* 93(1–4):505–513

Publisher's note Springer Nature remains neutral with regard to jurisdictional claims in published maps and institutional affiliations.